DINAME 2017 - Proceedings of the XVII International Symposium on Dynamic Problems of Mechanics
A. T. Fleury, D. A. Rade, P. R. G. Kurka (Editors), ABCM, São Sebastião, SP, Brazil, March 5-10, 2017

Dynamic Characterization and Efficiency Analysis of Multi Degree of Freedom Piezoelastic Energy Harvesters from Structural Vibrations

Akio Hanasiro[1], **Paulo S. Varoto**[1]

[1] Sao Carlos Engineering School, EESC-USP, Av. Trabalhador Saocerlense 400, Sao Carlos, 13566-590, SP, Brasil, akioha.mob@gmail.com, fcapucini@usp.br, varoto@sc.usp.br

Abstract: In the past decade considerable research efforts have been dedicated to the process of converting structural vibration signals into usable electric energy by employing piezoelectric materials, frequently referred to as piezoelectric energy harvesting (PEH). Base driven electromechanical single degree of freedom (SDOF) models such as the well known cantilever beam has inspired many relevant contributions in this area. Despite its versatility, SDOF presents limitations specially related to frequency tuning and bandwidth of operation. Multi degree of freedom (MDOF) models appeals as a valid modeling strategy to enhance the mechanical to electrical energy conversion process. The main goal of this article is to assess the feasibility and efficiency of employing MDOF models in the design of piezoelastic energy harvesters. A distributed parameter model is formulated of an L-shape harvester covered with segmented piezoceramics. Numerically simulated results have shown significant differences on the harvester's output electric energy power for different simulation scenarios where the amount of piezoelectric elements as well as their spatial distribution on the host structure were varied. Experimental tests were performed on a prototype and measured results were in good agreement with the corresponding simulated data.

Keywords: Piezoelectric Energy Harvesting, L-Shape Beams, Structural Vibrations, Harvesting Efficiency

INTRODUCTION

Recent technological developments in microelectronics and wireless areas demands for alternative energy sources capable of powering low power small electronics. Motivated by its ubiquitous essence, energy generation from environmental structural vibrations has been widely investigated among other renewable energy resources in last decades (Williams and Yates, 1996), where different applications potentials have been discussed and evaluated on the literature (Starner and Paradiso, 2004), (Zuo and Tang, 2013), comprising since human (Karami and Inman, 2012) body to vehicles and buildings vibration sources (Stephen, 2006). The usage of the piezoelectric transduction, commonly referred to as piezoelectric energy harvesting (Erturk and Inman, 2011) has also been subject of various investigations (Anton and Sodano, 2007), (Kim et al., 2011), (Calio et al., 2014), due to the simplicity and reduced package of available solutions (Beeby et al., 2006) when compared to other usual transduction mechanisms, e.g. electromagnetic and capacitive.

A common approach to maximize the energy harvesters power output duToit et al. (2005) is the usage of dynamic effects of resonance, designing the structure of the device to exhibit natural frequencies that are close to those of the vibration sources, maximizing the response amplitude, and thus the generated energy. However, in broadband random vibration applications the frequency tuning is a typical issue faced by energy harvesters, where the earlier cantilever solutions adopted, usually exhibiting a single resonant frequency on the operation frequency bandwidth, had very poor results due to its narrow band response amplification.

In this context, many different solutions have been proposed to increase the energy harvesters operation frequency bandwidth, ranging from induced nonlinearities to create bi or tri-stable states, using magnets, compressive preloads, or even mechanical stops (Mann and Owens, 2010), (Cottone et al., 2007), Daqaq et al. (2014) , to multiple-degree-of-freedom systems (Tang and Yang, 2015), (Tang et al., 2012), (Xiao et al., 2016), were more than one resonant frequency is found, enabling different approaches to raise power outputs on the resonance surroundings. Nevertheless, in some studies the multiple-degree-of-freedom energy harvesters are evaluated using only concentrated parameters models, where general results can be evaluated and discussed, but its applicability to a constructive solution have to be of concern. One very interesting and promising solution to multiple-degrees-of-freedom piezoelectric energy harvesting presented (Erturk et al., 2009a) is the L-shaped cantilevered configuration, which features an easy frequency tuning capability through the second lumped mass position.

However, most researches developed in piezoelectric energy harvesting focus on increasing efficiency and energy densities based only on the device total masses, neglecting the piezoelectric material demand of the evaluated solutions,

which can have significant impact on costs, and, consequently, market feasibility. The piezoelectric patch insertion between every oscillator proposed by Xiao (Xiao et al., 2016) , with no concern about each ones contribution to the total generated energy, or the widely adopted full piezoelectric covered cantilevers (Erturk et al., 2009a), (Erturk and Inman, 2008a), (Erturk and Inman, 2008b), Goldschmidtboeing and Woias (2008), that are known to exhibit non-uniform strains, are some good examples.

This article aim to expose a case study where through the identification and elimination of low efficiency piezoelectric segments the power output and the energy density of a energy harvester was improved, especially based on the piezoelectric material amount, serving as a guideline that can easily be adapted or replicated to optimize other cantilevered structures configuration.

The main goal of the present paper is to present results from an experimental analysis performed on a typical L-shape harvester containing segmented piezoelectric layers on both horizontal and vertical beams in order to investigate the phenomenon of modal interaction when the first two natural frequencies of the system are commensurable. For that purpose, a L-shape beam structure was designed such that the 2:1 ratio between these frequencies can be achieved. A linear dynamic model is derived and validated using modal analysis principles Ewins (2000). Experimental nonlinear tests were performed on the harvester in order to investigate the occurrence of modal interactions when the system is driven in either one of the commensurable resonant frequencies. Experimental results confirm the presence of modal interactions between the commensurable frequencies, and indicate that additional electrical energy can be harvested thus improving the performance of the harvesting device.

ELECTROMECHANICAL RESPONSE MODEL

In the present section the main theoretical aspects of the electromechanical modeling of the harvesting system studied are summarized. Figure 1a shows the proposed energy harvester that consists of a combination of two slender beams carrying lumped masses (M_1 and M_2) and connected in a L-shape geometry. The proposed harvester is similar to (Erturk et al., 2009a) and previously investigated in (Haddow et al., 1984) (Balachandran and Nayfeh, 1990), except that in the later work purely mechanical linear and nonlinear dynamic characteristics were studied. Recent work (Chen et al., 2016) also employs the L-shape geometry in the context of piezoelectric energy harvesting with similar induced nonlinear restoring mechanisms using magnets. According to Fig. 1a The horizontal beam is clamped at one end connected to M_1 at the other end. The vertical beam is fixed at M_1 and attached to M_2 at the free end. Both beams carry identical piezoelectric layers partially covering the beams and presenting cross section properties that are shown in Fig. 1a. Euler-

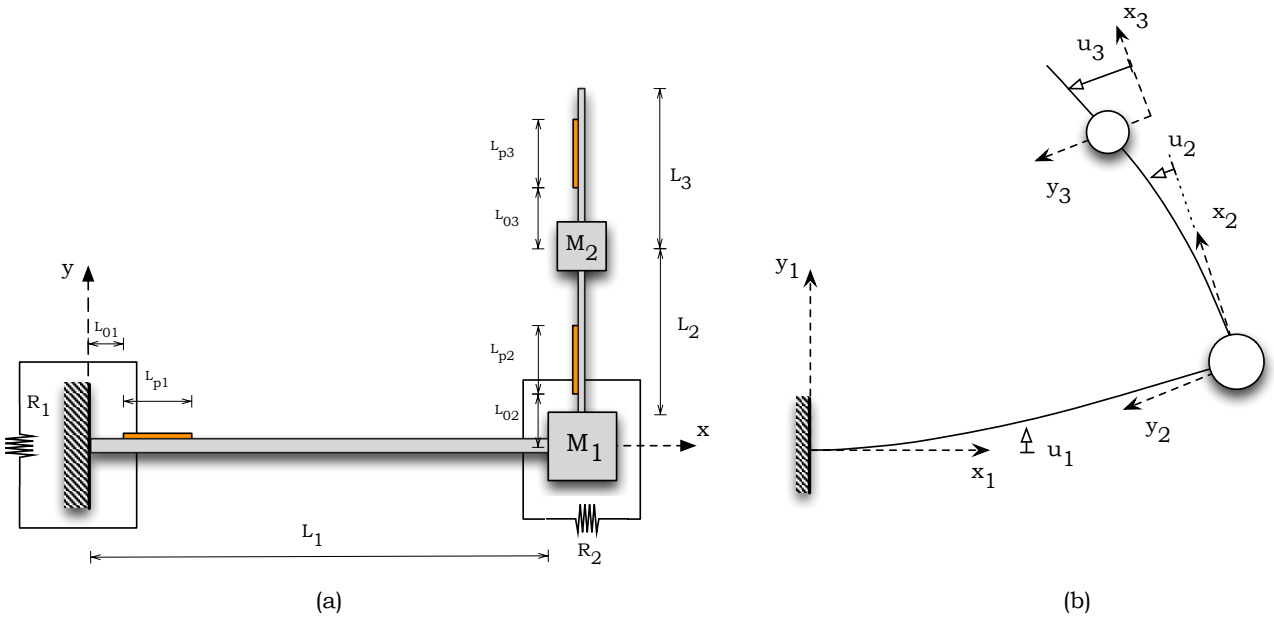

Figure 1 – (a) L-shaped beam piezoelectric harvester; (b) Reference frame

Bernoulli beam theory is used to obtain the time domain undamped electromechanical partial differential equations for

free vibration response for each beam segment shown in Fig. 1, and they can be expressed as

$$m_1 \frac{\partial^2 u_1(x_1,t)}{\partial t^2} + E_1 I_1 \frac{\partial^4 u_1(x_1,t)}{\partial x_1^4} + \vartheta_1 \upsilon_1(t) H_1(x_1) = 0 \tag{1}$$

$$m_2 \frac{\partial^2 u_2(x_2,t)}{\partial t^2} + E_2 I_2 \frac{\partial^4 u_2(x_2,t)}{\partial x_2^4} + M_2 g \frac{\partial^2 u_2(x_2,t)}{\partial^2 x_2^2} + \vartheta_2 \upsilon_2(t) H_2(x_2) = 0 \tag{2}$$

$$m_3 \frac{\partial^2 u_3(x_3,t)}{\partial t^2} + E_3 I_3 \frac{\partial^4 u_3(x_3,t)}{\partial x_3^4} + \vartheta_3 \upsilon_3(t) H_3(x_3) = 0 \tag{3}$$

where m_k, M_i, $E_i I_i$ are structural parameters of the k^{th} beam segment ($k = 1,...,3$), namely, the mass linear density (mass per unity of length), the lumped mass attached to each beam end and the bending stiffness. Equations 3 also incorporate the output voltages $\upsilon_1(t)$ of the piezoelectric layers and the coupling coefficient ϑ_i in physical coordinates. These voltage terms are multiplied by heaviside functions $H_i(x_i)$ ($H_i(x_i) = H(x_i - L_{0i}) - H(x_i - l_{0i} - L_{pi})$) due to the fact that the harvester model shown in Fig. 1 employs segmented piezoelectric layers not covering the entire length of each beam segment. Figure 1a and 1b also show additional geometric and electric parameters of the energy harvesting system and 1b shows the reference frame that define the spatial displacement coordinates of for the system under consideration.

Free Undamped Response

Neglecting the effects of shear deformation and rotary inertia on the bending vibration, the well known Euler-Bernoulli beam model (Rao, 2007) is employed in the present analysis in order to obtain the undamped natural frequencies and natural eigenfunctions of the structure under investigation. The free undamped motion of each beam segment shown in Fig. 1 can be describe in terms of a summation of eigenfunctions according to the principle of linear superposition (Clough and Penzien, 2003)

$$u_k(x,t) = \sum_{p=1}^{N} \phi_{kp}(x)\eta_p(t) \qquad r = 1,...3 \tag{4}$$

where $\phi_{kp}(x)$ and $\eta_p(t)$ are the piecewise eigenfunction and time domain modal response corresponding to the p^{th} vibration mode, respectively. The eigenfunctions are defined as (Rao, 2007)

$$\phi_{1p}(x_1) = A_{1p}\sin(\alpha_p x_1) + B_{1p}\cos(\alpha_p x_1) + C_{1p}\sinh(\alpha_p x_1) + D_{1p}\cosh(\alpha_p x_1) \tag{5}$$

$$\phi_{2p}(x_2) = A_{2p}\sin(\beta_p x_2) + B_{2p}\cos(\beta_p x_2) + C_{2p}\sinh(\gamma_p x_2) + D_{2p}\cosh(\gamma_p x_2) \tag{6}$$

$$\phi_{3p}(x_3) = A_{3p}\sin(\mu_p x_3) + B_{3p}\cos(\mu_p x_3) + C_{3p}\sinh(\mu_p x_3) + D_{3p}\cosh(\mu_p x_3) \tag{7}$$

where coefficients α_p, β_p, γ_p, and μ_p are the eigenvalues related to the system's undamped natural frequencies and A_{ip} and B_{ip} are the coefficients of the eigenfunctions that correspond to the undamped natural modes of vibration of the piecewise beams segments. Application of proper geometric boundary conditions for the clamped end at $x_1 = 0$ and force/moment equilibrium relationships between M_1 and M_2 at $x_1 = L_1$ and $x_2 = 0$ and beam segment 3 and M_2 at $x_3 = 0$, the undamped natural frequencies and eigenfunctions can be obtained. Further analytical details of this procedure can be found in references (Rao, 2007) and (Erturk et al., 2009a). It should be noticed that the undamped natural frequencies are calculated for the short circuit conditions of the energy harvesting circuit, i.e. when $R_l \to 0$, where R_l is the circuit load resistance.

0.1 Forced Damped Transmissibility Response

As shown in Fig. 1 the input to the L-shape energy harvester considered is given by the base displacement $u_b(x_1 = 0,t)$. This excitation imposes a distributed inertial loading to the harvester's resulting in bending motions in the $x-y$ plane. According to Eqs. 3 only the beam segment corresponding to $k = 1$ is affected by this base driven input motion. However, the coupling between both beams segments through the right angle connection at M_2 will force all the structure to exhibit bending vibrations in responde to the inertial loading. Two mechanical output responses are of particular interest in the present analysis, the vertical motion of M_1 at $x_1 = L_1$ and the horizontal motion at M_2 at $x_2 = L_2$. Similarly, the output electrical voltages from the horizontal and vertical piezoelectric layers correspond to the electrical output from the energy harvesting circuit. Once these four quantities are determined, mechanical and voltage transmissibility frequency response functions can be obtained considering a constant amplitude and varying frequency harmonic input motion. In modal coordinates the p^{th} equation of motion is given as (Erturk et al., 2009a)

$$\frac{\mathrm{d}^2\eta_p(t)}{\mathrm{d}t^2} + 2\zeta_p\omega_p^2 + \frac{\mathrm{d}\eta_p(t)}{\mathrm{d}t} + \omega_p^2\eta_p(t) + \sum_{k=1}^{3}\chi_{kp}\upsilon_k(t) = Q_p(t) \tag{8}$$

where ζ_p is the viscous damping ratio of the p^{th} vibration mode υ_k is the output voltage across the electrodes of k^{th} beam segment, χ_{kp} is the modal electromechanical coupling term and $Q_p(t)$ is the modal forcing function that are given according to the following relationships

$$\chi_{kp} = \vartheta \frac{\mathrm{d}\phi_{kp}(x_k)}{\mathrm{d}x_k}\bigg|_0^{x=L_{pk}} \tag{9}$$

$$Q_p(t) = -\left(m_1 \int_0^{L_1} \phi_{1p}(x_1)\,\mathrm{d}x_1 + M_\mathrm{t}\phi_{1p}(L_1) \right) \ddot{u}_b(t) \tag{10}$$

where $M_t = M_1 + M_2 + m_2 L_2 + m_3 L_3$ and $\ddot{u}_b(t) = \ddot{u}_b(x_1 = 0, t)$ is the input acceleration imposed to the system's boundary at $x_1 = 0$. The modal damping ratio ζ_p is assumed to be a combination of strain-rate and viscous damping mechanisms and given as (Franco, 2013). Assuming harmonic variations for the quantities shown in Eq. 8

$$\ddot{u}_b(x_1 = 0, t) = U_b \mathrm{e}^{j\omega t}$$
$$\eta_{r_p}(t) = H_p \mathrm{e}^{j\omega t} \tag{11}$$
$$\upsilon_k(t) = V_k \mathrm{e}^{j\omega t} \tag{12}$$

where U_b is the amplitude of the input base acceleration and H_p and V_k are the complex valued amplitudes of the mechanical response in modal coordinates and the k_{th} piecewise output voltage from each piezoelectric layer. For a unit amplitude of the input motion $H_p(\omega)$ These two last quantities are evaluated as

$$H_p(\omega) = \frac{\lambda_p - \sum_{k=1}^{3} \chi_{kp} V_k}{\omega_p^2 - \omega^2 + j2\zeta_p \omega_p \omega} \tag{13}$$

$$\lambda_p(t) = -\left(m_1 \int_0^{L_1} \phi_{1p}(x_1)\,\mathrm{d}x_1 + M_\mathrm{t}\phi_{1p}(L_1) \right) \tag{14}$$

Following a similar procedure as in (Erturk et al., 2009a) the frequency domain complex valued output voltages V_k are evaluated from the solution of a system of linear equations for each value of the excitation frequency according to

$$\sum_{k=1}^{3} G_{mk} V_k = T_m \; m = 1..., 3 \tag{15}$$

$$G_{mk}(\omega) = \frac{1}{R_l} + j\omega (C_p)_m \delta_{mk} + \sum_{p=1}^{2} \frac{j\omega \psi_{mp} \chi_{kp}}{\omega_p^2 - \omega^2 + j\omega 2\zeta_p \omega_p \omega} \tag{16}$$

$$T_m(\omega) = \sum_{p=1}^{2} \frac{j\omega \psi_{mp} \lambda_p}{\omega_p^2 - \omega^2 + j\omega 2\zeta_p \omega_p \omega} \tag{17}$$

with

$$\psi_{kp} = -(d_{31})_k (E_p)_k (h_{pc})_k b_k \frac{\mathrm{d}\phi_{kp}(x_k)}{\mathrm{d}x_k}\bigg|_0^{L_k} \tag{18}$$

Solution of the system of equations expressed in Eq. 15 give the output voltage for each individual piezoelectric layer. The total voltage for the series connection can be easily obtained by summing the V_k for each layer where the mode cancelation phenomenon (Erturk et al., 2009b) must be accounted for. Equations 13 and 15 were obtained by assuming a unit magnitude of the acceleration input motion, i.e. $A_b = 1$. Hence $H_p(\omega)$ and $V_k(\omega)$ as obtained from these expressions correspond to the acceleration transmissibility FRFs that will be required in further developments.

Once the individual voltages are calculated from the solution of Eq. 15 the total output voltage and electric power transmissibility FRF are determined for a series connection of the piezoelectric layers according to

$$V = \sum_{k=1}^{3} V_k \tag{19}$$

$$P = \frac{\|V\|^2}{R_l} \tag{20}$$

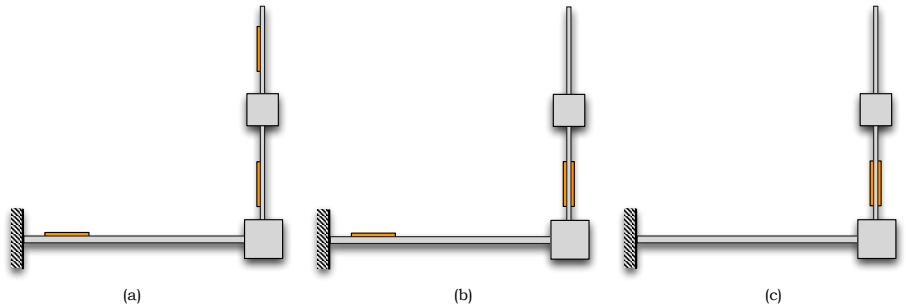

Figure 2 – Three different geometric configurations of the energy harvesting system used in numerical simulations.

NUMERICAL SIMULATIONS

Numerical simulations for the L-shaped energy harvester model derived in the previous section were conducted for the three different configurations shown in Fig. 2. The first simulation scenario shown in Fig. 2a is referred to as the baseline configuration in which the energy harvesting system contains three piezoelectric segmented layers, one at the top surface of the horizontal beam segment and two on the inner surface of the vertical beam. This configuration is similar to the energy harvesting system studied by Erturk et al. (2009a). As seen from Figs. 2b and 2c the remaining simulation scenarios present variations on the position and quantity of piezoelectric layers that were employed on the harvesting system. For all three cases shown in Fig. 2 the length of the piezoelectric patches, the position of the lumped mass M_2 on the vertical beam and value of the load resistance R_l were varied over a wide range and for all cases the electric power transmissibility FRF were calculated according to Eqs. 19 and 20. In all numerical simulations was assumed that the base driven input acceleration had a magnitude of 1 $m.s^{-2}$. Numerical values for the geometrical parameters as well as material properties used in the numerical simulations are presented in Table 1.

Table 1 – L-Shaped Model Parameters

Parameter	Value	Unit
L_1	190	mm
$L_2 + L_3$	220	mm
L_{pk} [1]	38.1	mm
h_{s1}	3	mm
h_{s2}	1.5	mm
h_p	0.05	mm
b_s	25	mm
b_p	20.6	mm
M_1	71	g
M_2	38	g
ρ_s	7870	kg/m3
ρ_p	7800	kg/m3
d_{31}	-190	pm/V
ε_{33}^S	-13.27	nF/m
Y_s	207	GPa
Y_p	60.6	GPa

The first simulation was carried out for the baseline configuration of Fig. 2a. First, M_2 was fixed at a position corresponding to $L_2 = 108.9\ mm$ and the length of the horizontal and first vertical piezoelectric layers were maintained constant while the length of the third piezoelectric layer on the free portion of the vertical beam was varied. Results of this simulation are presented on Fig. 3, where each figure shows the electrical power transmissibilty FRF to a unit value of the input base acceleration.

Results depicted on Fig. 3 were obtained for the vibration mode opposite to the mode where cancelation due to mismatched polarity of electrical signals occur, as explained in Erturk et al. (2009b). It can be clearly seen from this first simulation result that an increase on the piezoelectric lenght on the third beam segment do not increase the output electrical power in the same rate. Instead, depending on the resonant frequency and the cancelation configuration, the increase in piezoelectric amount may cause the power output to be reduced. Extending the investigation by varying the position of M_2 on the vertical beam segment it is seen from Fig. 4 that observed that in most configurations the maximum output power is not achieved for the full covered segment case. The next simulation scenario corresponds to the geometry shown in Fig. 2b. In this case the piezoelectric layer on L_3 was removed and an aditional layer is considered on L_2 on the outer side of the vertical beam segment, thus forming a bimorph geometrical configuration for the vertical beam. Results are shown in Fig. 5. It can be noticed that the results obtained from the simulation using the second configuration follow the same

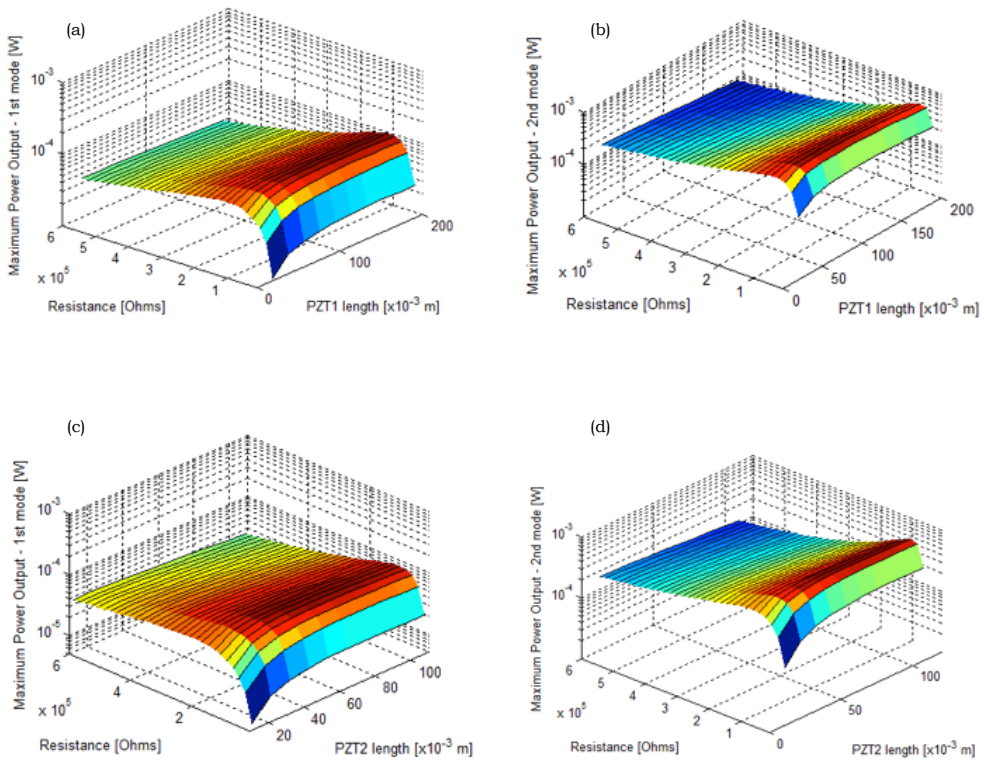

Figure 3 – Electrical power FRF transmissibility FRF for the baseline configuration: (a) first segment, with cancelation on second mode, (b) first segment with cancelation on the first mode, (c) second segment, with cancelation on second mode, (d) second segment, with cancelation on the first mode.

trends observed in the simulation of the baseline energy harvesting system, except that in the present case higher levels of the resulting electric power are obtained with the same amount of piezoelectric material just by varying the location of the third piezoelectric layer on the vertical beam segment. This increase on the performance of the second configuration when compared with the baseline configuration was expected since the bimorph geometry shown from Fig. 2b is located on a position of maximum strain rates on the vertical beam segment thus maximizing the values of the first derivative of the mode shapes in Eq. 18 and consequently having a positive effect on the calculation of the electric power. Finally, the simulation results for the third configuration shown in Fig. 2c are shown in Fig. 6. In thi case the second resonant frequency was considered for different values of the geometric properties. The absence of mode cancelation in the results shown in Fig. 6 demonstrate that the third configuration is promissing as far as the resulting amount of electrical power is concerned, showng an increase of up to twice the amount of output voltage when compared to the baseline configuration.

EXPERIMENTAL VALIDATION

Using a prototype of the L-shaped piezoelectric energy harvester, laboratory experiments were conducted to validate the theoretical model used to conduct the case study optimization. The three investigated configurations were tested and the measured responses were compared to the numerically predicted ones, using different resistance values and cancelation modes to ensure that the mathematical model accurately represents the physical phenomena in all situations. Figure 7 shows the experimental arrangement that was used to measure the harvester's output electromechanical voltage transmissibility FRF. The L-shaped prototype was manufactured using carbon steel for the cantilevered beam segments, with lengths of $L_1 = 192$ mm and $L_2 = 182mm$ for the first and second beam, respectively, and thickness of 1.65 mm and 2.50 mm, with partial cover piezoelectric patches positioned close to each segment origin. Aluminum blocks were used to represent the lumped masses and constraint the structure segments to each other, with the second mass positioned at half length of the second beam. The harvester structure was rigidly attached to an electromechanical shaker, used to apply a random mechanical load. The experiments were conducted using two different resistance values ($100k\Omega$ and $500k\Omega$) for the three configurations discussed along the optimization, and both modes cancelation for the first and second configuration. The frequency response function of the harvester voltage output was obtained comparing the measured voltage at the resistance poles with the applied acceleration at the structure base. The accelerations on the first and second lumped masses were also evaluated to validate the structure mode shapes. Figure 8a and 8b show the resulting measured and calculated voltage transmissibiity FRF for configurations 1 and 2 from Fig. 2. An excelent agreement is observed bwtween numerically calculated and experimental results what indicates that the numerical model used in the present study is valid for designing and simulation of further configurations scenarios of the energy harvesting system.

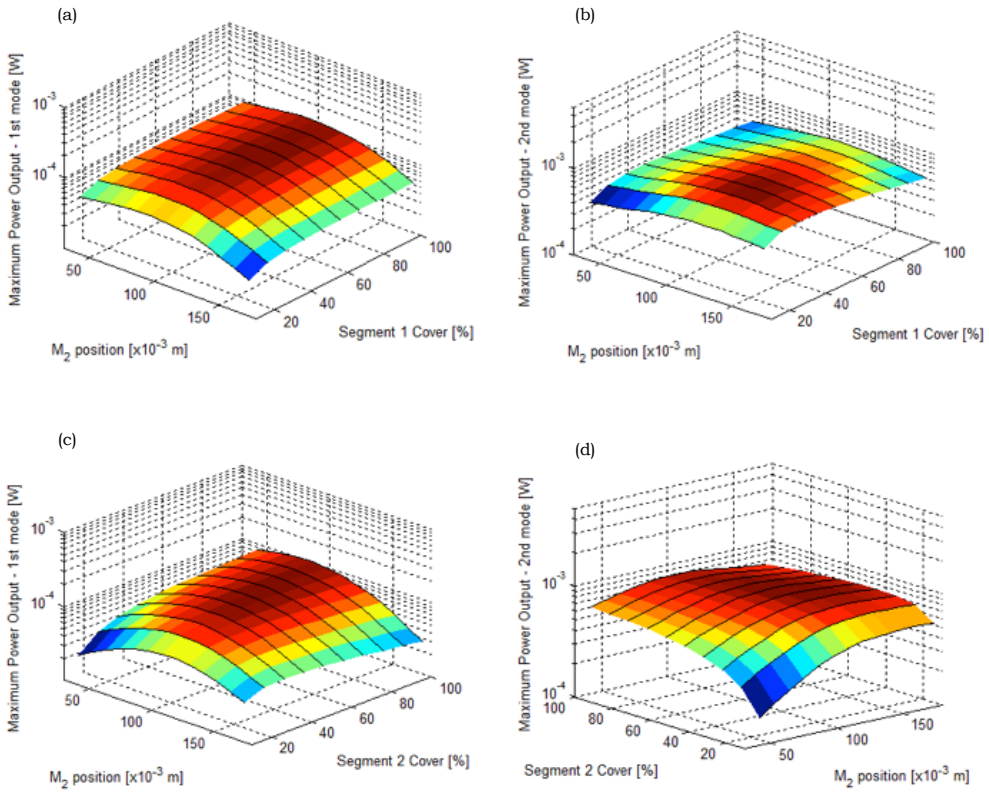

Figure 4 – Maximum power output for the baseline configuration for different positions of M_2 and varying the piezoelectric patch length of: (a) first segment, with cancelation on second mode, (b) first segment with cancelation on the first mode, (c) second segment, with cancelation on second mode, (d) second segment, with cancelation on the first mode.

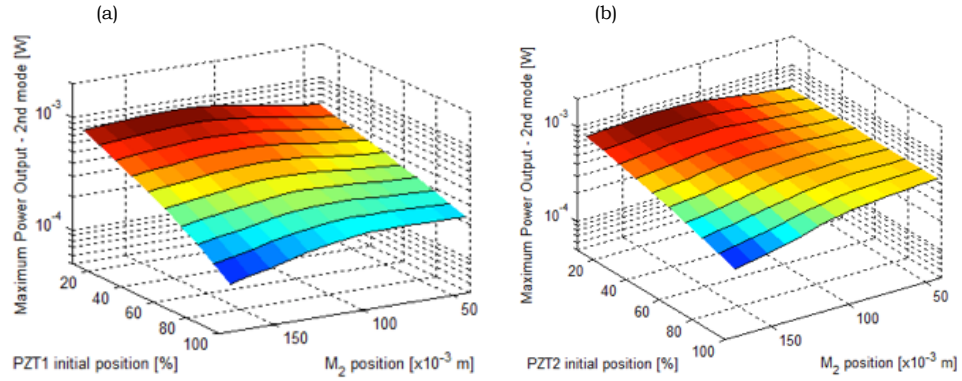

Figure 5 – Maximum power output obtained for the second configuration on the second resonant frequency, for different M2 positions and varying the second segment piezoelectric patch (a) length and (b) initial position, with cancelation on the first mode.

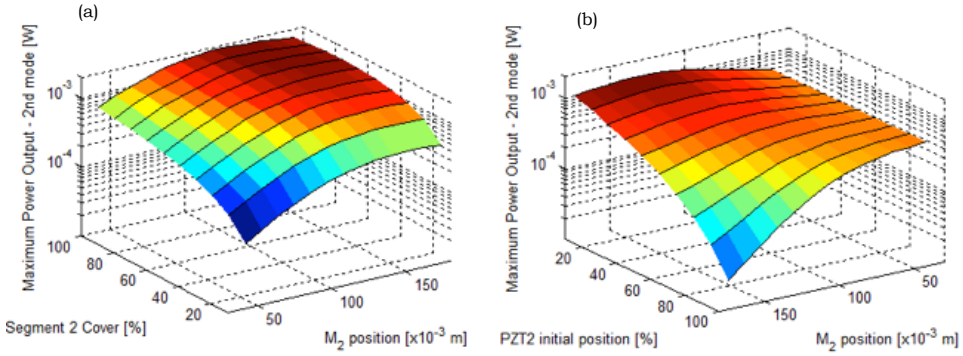

Figure 6 – Maximum power output obtained for the third configuration on the second resonant frequency, for different M_2 positions and varying the second segment piezoelectric patch (a) length and (b) initial position.

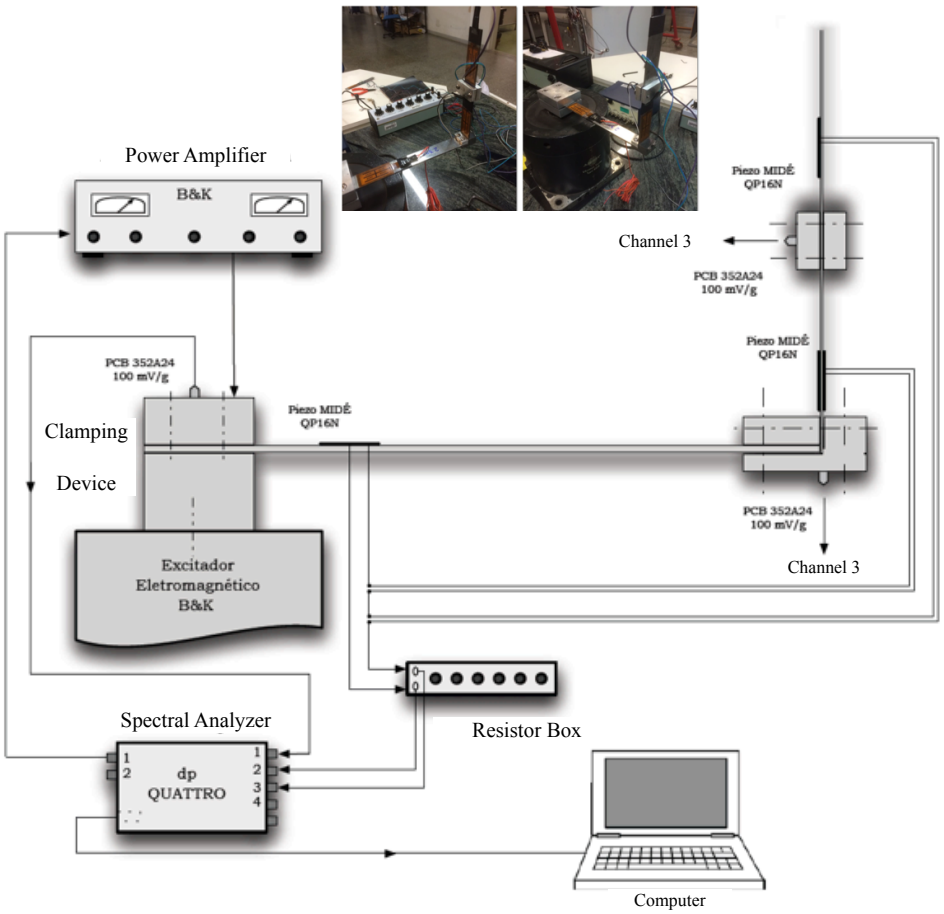

Figure 7 – Laboratory test setup and actual experiment performed to validate the energy harvesting dynamic model

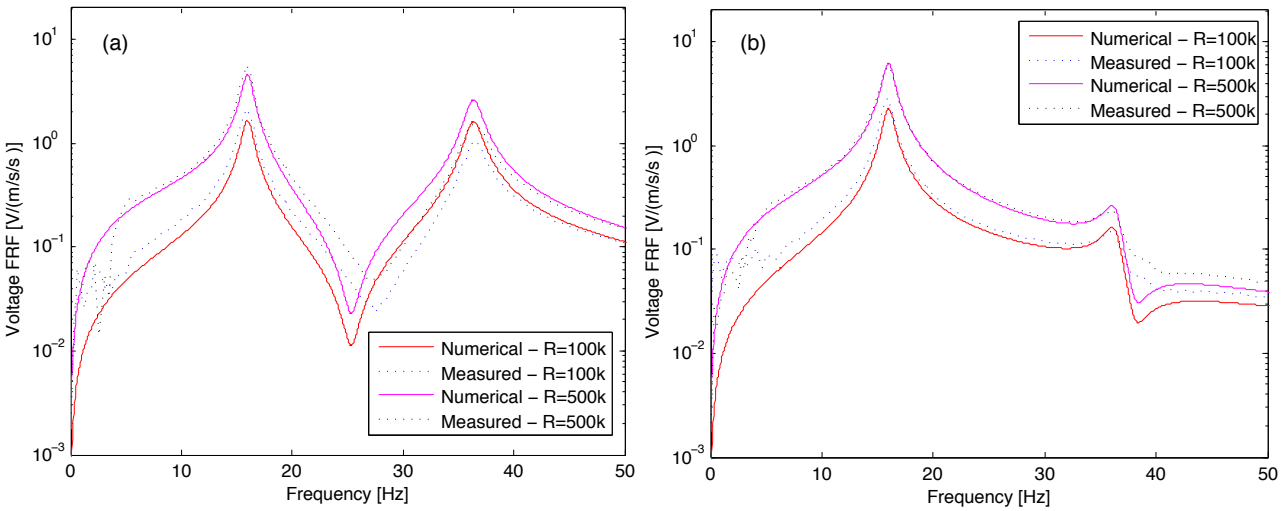

Figure 8 – Measured and simulated results for different values of the load resistance: (a) configuration 1 ; (b) configuration 2

CONCLUSIONS

In this article the efficiency of a multi-degree-of-freedom piezoelectric energy harvester was discussed using a case study of the L-shaped constructive solution. It was shown through a brief critical review of the theoretical basis and various sensitivity analysis that the nonselective insertion of piezoelectric material may not only have very low contributions to the power output increase, but causes the response to be reduced, resulting in an harvester efficiency detriment for both cases. These consequences are also more significant when evaluating the energy density in terms of piezoelectric material quantity, very meaningful when costs compromises are involved. A two-step optimization example was presented, were at first the energy density was improved through the selective positioning of the piezoelectric elements in higher potential segment regions. Secondly the efficiency was increased through the elimination of the cancelation effect due to series connection between two opposite potential piezoelectric elements, observed on the first and second beam segments. Other possible solutions for increasing harvester efficiency, as more complex electrical circuits were not discussed, where costs compromises have also to be of concern. The theoretical model was experimentally validated using an L-shaped energy harvester prototype with very good agreement between measured and simulated results, granting a high confidence level to the investigation performed.

ACKNOWLEDGMENTS

The authors recognize and acknowledge all academic and laboratory support received from EESC-USP to the development of this work.

REFERENCES

S. R. Anton and H. A. Sodano. A review of power harvesting using piezoelectric materials (2003-2006). *Smart Materials and Structures*, 16(3):1–21, 2007.

B. Balachandran and A.H. Nayfeh. Nonlinear motions of beam-mass structure. *Nonlinear Dynamics*, 1:39–61, 1990.

S. P. Beeby, M. J. Tudor, and N. M. White. Energy harvesting vibration sources for microsystems applications. *Measurement Science & Technology*, 17(12):175–195, 2006.

R. Calio, U. B. Rongala, D. Camboni, C. Stefani, G. De Petris, and C. M. Oddo. Piezoelectric energy harvesting solutions. *Sensors*, 14(3):4755–4790, 2014.

L. Chen, W. Jiang, M. Panyam, and M.F. Daqaq. A broadband internally resonant vibratory energy harvester. *Journal of Vibration and Acoustics*, 138(6):1–10, 2016.

R. Clough and J. Penzien. *Dynamics of Structures*. Computers & Structures, third edition, 2003.

F. Cottone, L. Gammaitoni, H. Vocca, M. Ferrari, and V. Ferrari. Piezoelectric buckled beams for random vibration energy harvesting. *Smart Materials and Structures*, 21(3):035021, 2007.

M. F. Daqaq, R. Masana, A. Erturk, and D. D. Quinn. On the role of nonlinearities in vibratory energy harvesting: A critical review and discussion. *Applied Mechanics Reviews*, 66(4):1–23, 2014.

N. E. duToit, B. L. Wardle, and S. G. Kim. Design considerations for mems-scale piezoelectric mechanical vibration energy harvesters. *Integrated Ferroelectrics*, 71(1):121–160, 2005.

A. Erturk and D. J. Inman. A distributed parameter electromechanical model for cantilevered piezoelectric energy harvesters. *Journal of Vibration and Acoustics*, 130:1–15, 2008a.

A. Erturk and D. J. Inman. On mechanical modeling of cantilevered piezoelectric vibration energy harversters. *Journal of Intelligent Material Systems and Structures*, 18(10):1311–1325, 2008b.

A. Erturk and D. J. Inman. *Piezoelectric Energy Harvesting*. Wiley, first edition, 2011.

A. Erturk, J.M. Renno, and D.J. Inman. Modeling of piezoelectric energy harvesting from an l-shaped beam-mass structure with an application to uav's. *Journal of Intelligent Material Systems and Structures*, 20(1):529–544, 2009a.

A. Erturk, P.A. Tarazaga, J.R. Farmer, and D.J. Inman. Effect of strain nodes and electrode configuration on piezoelectric energy harvesting from cantilevered beams. *Journal of Vibration and Acoustics*, 130:1–10, 2009b.

D. J. Ewins. *Modal Testing: Theory, Practice and Applications*. RSP, first edition, 2000.

V. R. Franco. *Optimization Techniques Applied to Piezoelectric Vibration Energy Harvesting Systems*. PhD thesis, Sao Carlos School of Engineering, University of Sao Paulo, Brazil, 2013.

F. Goldschmidtboeing and P. Woias. Characterization of different beam shapes for piezoelectric energy harvesting. *Journal of Micromechanics and Microengineering*, 18(10):1–13, 2008.

A.G. Haddow, A.D.S. Barr, and D.T. Mook. Theoretical and experimental study of modal interaction in a two-degree-of-freedom structure. *Journal of Sound and Vibration*, 97(3):451–473, 1984.

M. A. Karami and D. J. Inman. Powering pacemakers from heartbeat vibrations using linear and nonlinear energy harvesters. *Applied Physics Letters*, 100(4):1–4, 2012.

H.S. Kim, J. H. Kim, and J. Kim. A review of piezoelectric energy harvesting based on vibration. *International Journal of Precision Engineering and Manufacturing*, 12(6):1129–1141, 2011.

B. P. Mann and B. A Owens. Investigations of a nonlinear energy harvester with a bistable potential well. *Journal of Sound and Vibration*, 329(9):1215–1226, 2010.

S. Rao. *Vibrations of Continuous Systems*. Wiley, 2007.

T. Starner and J. Paradiso. *Human Generated Power for Mobile Electronics*, volume 1, chapter 45. CRC PRESS, 2004.

N. G. Stephen. On energy harvesting from ambient vibration. *Journal of Sound and Vibration*, 293(1-2):409–425, 2006.

L. Tang and Y. Yang. A multiple-degree-of-freedom piezoelectric energy harvesting model. *Journal of Intelligent Material Systems and Structures*, 23(14):1631–1647, 2015.

L. Tang, Y. Yang, and H. Wu. Modeling and experiment of a multiple-dof piezoelectric energy harvester. In *Proceedings of SPIE-Active and Passive Smart Structures and Integrated Systems*, 8341, pages 1–13, 2012.

C. B. Williams and R. B. Yates. Analysis of a micro-electric generator for microsystems. *Sensors and Actuators A*, 52 (1-3):8–11, 1996.

H. Xiao, X. Wang, and S. John. A multi-degree of freedom piezoelectric vibration energy harvester with piezoelectric elements inserted between two nearby oscillators. *Mechanical Systems and Signal Processing*, 68(1):138–154, 2016.

L. Zuo and X. D. Tang. Large-scale vibration energy harvesting. *Journal of Intelligent Material Systems and Structures*, 24(11):1405–1430, 2013.

RESPONSIBILITY NOTICE

The authors are the only responsible for the material included in this paper.